SUPPORTING INFORMATION

Inferring changes in summertime surface ozone-NO_x-VOC chemistry over U.S. urban areas from two decades of satellite and ground-based observations

Xiaomeng Jin[1,2], Arlene Fiore[1,2], K Folkert Boersma[3,4], Isabelle De Smedt[5], Lukas Valin[6]*

1. Department of Earth and Environmental Sciences, Columbia University, New York, NY, USA
2. Lamont-Doherty Earth Observatory of Columbia University, Palisades, NY, USA
3. Royal Netherlands Meteorological Institute, De Bilt, The Netherlands
4. Wageningen University, Environmental Sciences Group, Wageningen, The Netherlands
5. Belgian Institute for Space Aeronomy (BIRA-IASB), Brussels, Belgium
6. U.S. EPA Office of Research and Development, Research Triangle Park, NC, USA

Number of pages: 16

Number of figures: 17

S1. Satellite Retrieval of NO_2 and HCHO

We use multi-satellite products of daily tropospheric NO_2 and HCHO vertical columns accessed from the QA4ECV project (http://www.qa4ecv.eu/ecvs). The Differential Optical Absorption Spectroscopy (DOAS) method has been applied to retrieve NO_2 and HCHO column densities from spectral measurements at UV and visible wavelengths.[1] The retrieval of tropospheric NO_2 vertical column includes three steps:[2] 1) retrieval of the total slant column density along the optical path; 2) subtraction of the stratospheric NO_2 slant column (assimilation in the TM5-MP model) from the total slant column density;[3,4] 3) conversion of the tropospheric slant column density to vertical column density using air mass factors obtained from radiative transfer calculations that account for the viewing geometry, *a priori* vertical profiles of NO_2, and the presence of clouds and surface properties.[2,5] The retrieval of HCHO vertical column also involves retrieving the slant column and calculating air mass factors.[6] Improved spectral fitting algorithms are applied to the retrieval of slant column densities of NO_2 and HCHO, which has been shown to significantly reduce the errors of spectral fitting.[7] To reduce the latitude-dependent biases, HCHO slant columns are first adjusted using a two-step normalization with reference to background columns in the remote Pacific Ocean, where methane oxidation is assumed to be the only source of HCHO.[6] The *a priori* vertical profiles used for HCHO and NO_2 retrievals are obtained daily from TM5-MP chemical transport model simulations at 1°×1° degree resolution.[4]

S2. Gridding of Satellite Products

To grid satellite observations to a regular Cartesian grid, we calculate the area-weighted average:

$$\overline{\Omega}_{x,t} = \frac{\sum_t \sum_x w_i \times \Omega_i}{\sum_t \sum_x w_i} \quad \text{(S1)}$$

where Ω_i is the retrieved column density of each observation that overlaps with the grid cell *x* at a given temporal scale, and w_i is the overlapping area. While the target grid is smaller than the footprint of satellite observation, since the locations of the daily observations shift, a finer spatial resolution can be achieved by averaging over multiple time periods (a.k.a. spatial over-sampling).[8,9]

S3. Choice of Resolution

The choice of the coarse and fine horizontal resolution is subjective. To harmonize Ω_{NO2}, we use 0.125°× 0.125° as the fine resolution, which captures the spatial heterogeneity of NO_2 within urban areas.[10] After comparing the difference between OMI Ω_{NO2} and SCIAMACHY Ω_{NO2} at four different coarse resolutions, we selected 2 ° × 0.5° as the coarse resolution at which the difference is mostly systematic (Figure S1). Furthermore, we do not observe any significant temporal trends in $\Delta\Omega_{NO2\_Coarse}$ at 2° × 0.5°, indicating that we can use the long-term climatology of $\Delta\Omega_{NO2\_Coarse}$ to adjust SCIAMACHY Ω_{NO2} for the years with no OMI observations.

Supplementary Figures

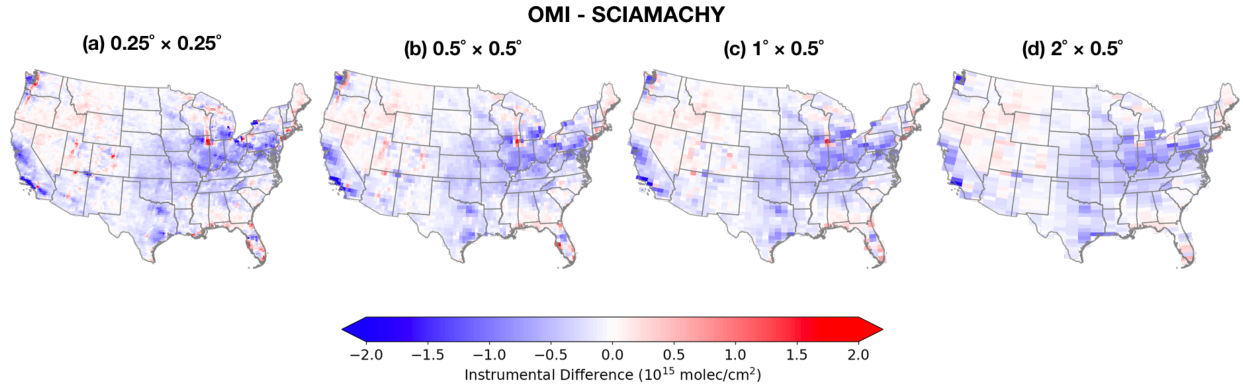

Figure S1. Difference between summertime average OMI Ω_{NO2} and SCIAMACHY Ω_{NO2} during the overlap period from 2005 to 2012 ($\overline{\Delta\Omega_{NO2\_Coarse}}(x_c, m)$, Equation 2) at multiple resolutions: (a) 0.25°× 0.25°; (b) 0.5°× 0.5°; (c) 1°× 0.5°; (d) 2°× 0.5°.

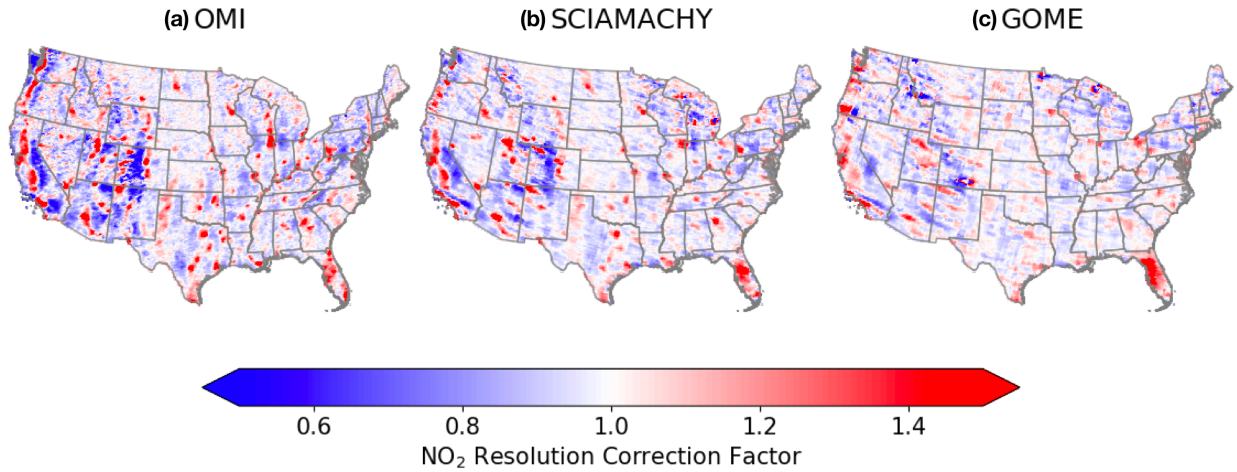

Figure S2. Resolution correction factor for Ω_{NO2} (RC_{NO2}) retrieved from (a) OMI, (b) SCIAMACHY, and (c) GOME. RC_{NO2} is estimated as the ratio of long-term summertime average Ω_{NO2} at a fine-resolution (0.125˚× 0.125˚) to that at a coarse resolution (2˚ × 0.5˚). We first grid satellite products to fine and coarse resolution grids by calculating area-weighted averages (Equation S1).

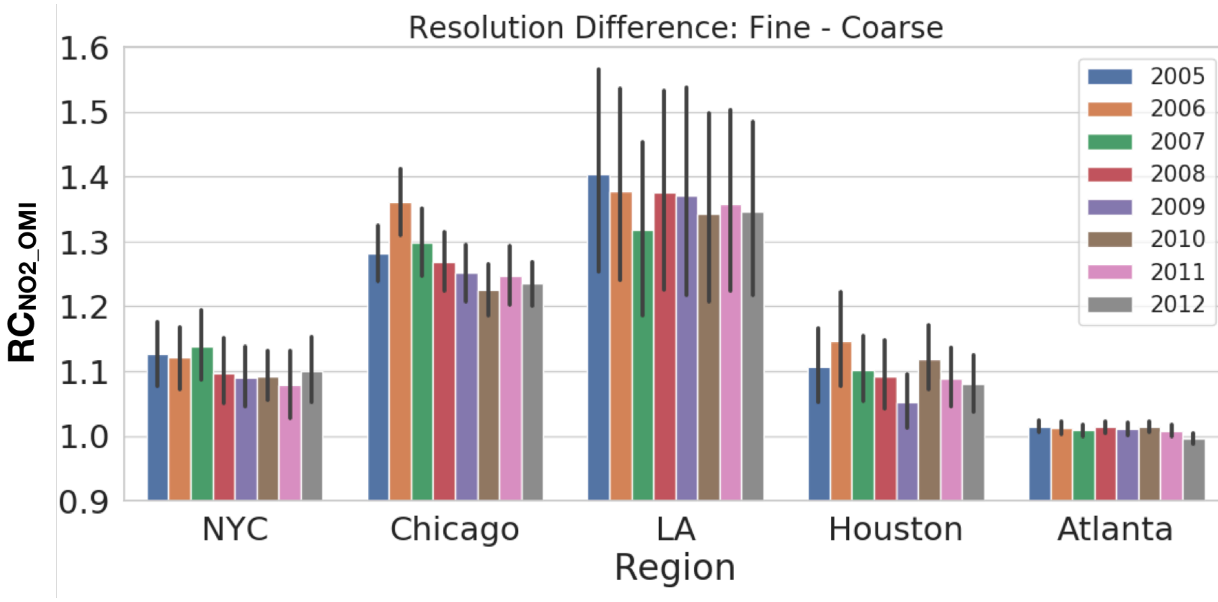

Figure S3. Year-to-year variability in summertime RC_{NO2_OMI} for five cities from 2005 to 2012. The error bars represent the spatial variations within each metropolitan area.

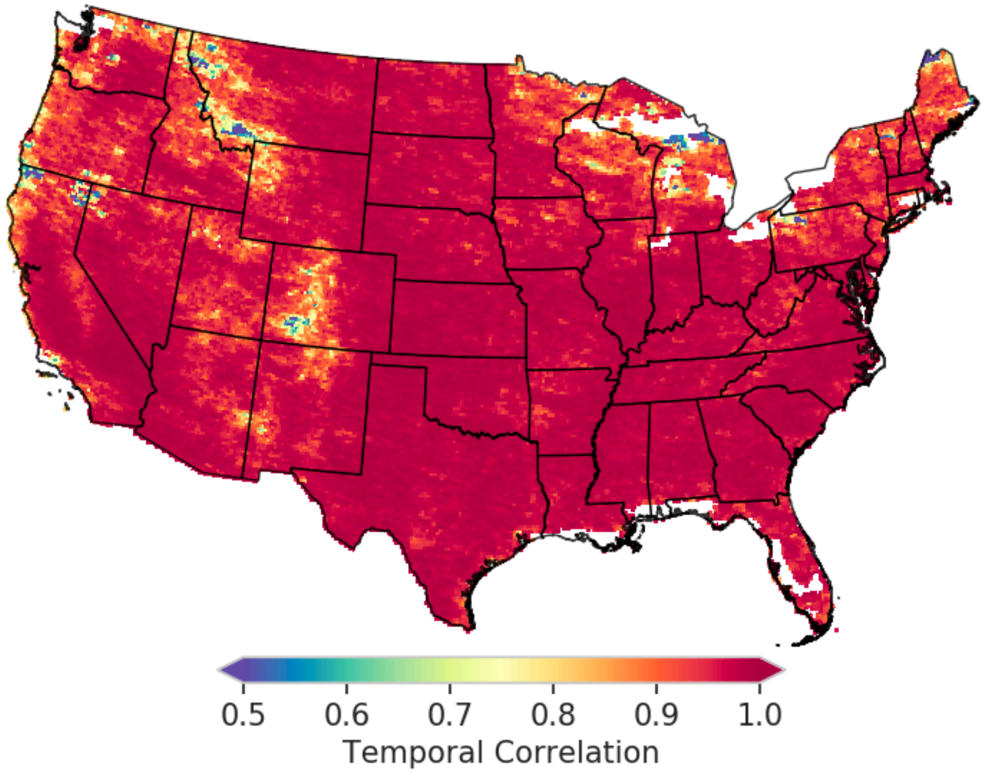

Figure S4. Temporal correlation (Pearson correlation coefficient R) between RC_{NO2_OMI} and RC_{NO2_SCIA} during the overlap period. The temporal correlation is calculated monthly for June, July and August from 2005 to 2012. White space indicates insufficient data to calculate R value.

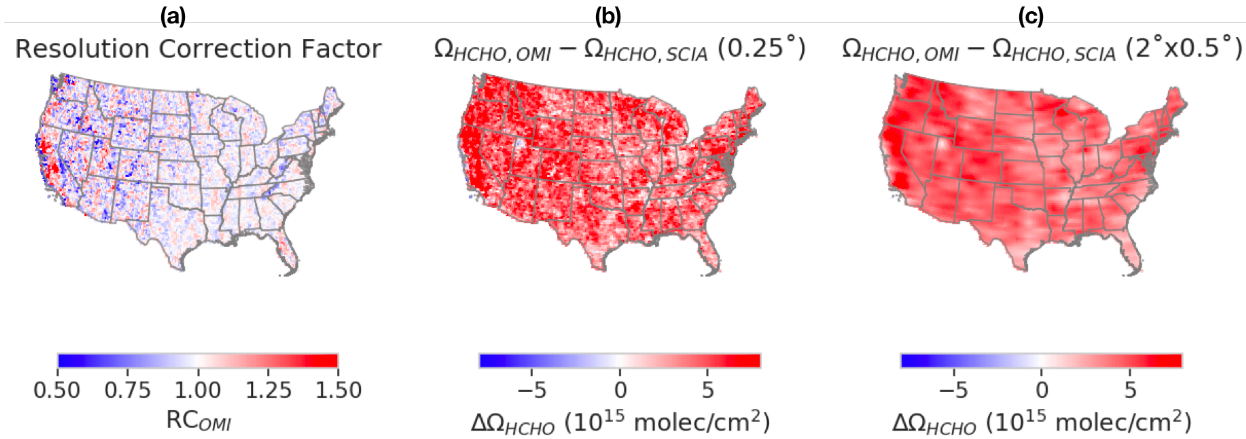

Figure S5. (a) Resolution correction of OMI Ω_{HCHO} (RC_{HCHO_OMI}) factor, which is estimated as the ratio of the long-term summertime average Ω_{HCHO} on a fine-resolution (0.25°× 0.25°) to that on a coarse-resolution (2° × 0.5°) grid. (b) Difference between summertime average OMI Ω_{HCHO} and SCIAMACHY Ω_{HCHO} during the overlap period ($\overline{\Delta\Omega_{HCHO}}(x_c, m)$, Equation 8) at (b) 0.25°× 0.25°and (c) 2°× 0.5°.

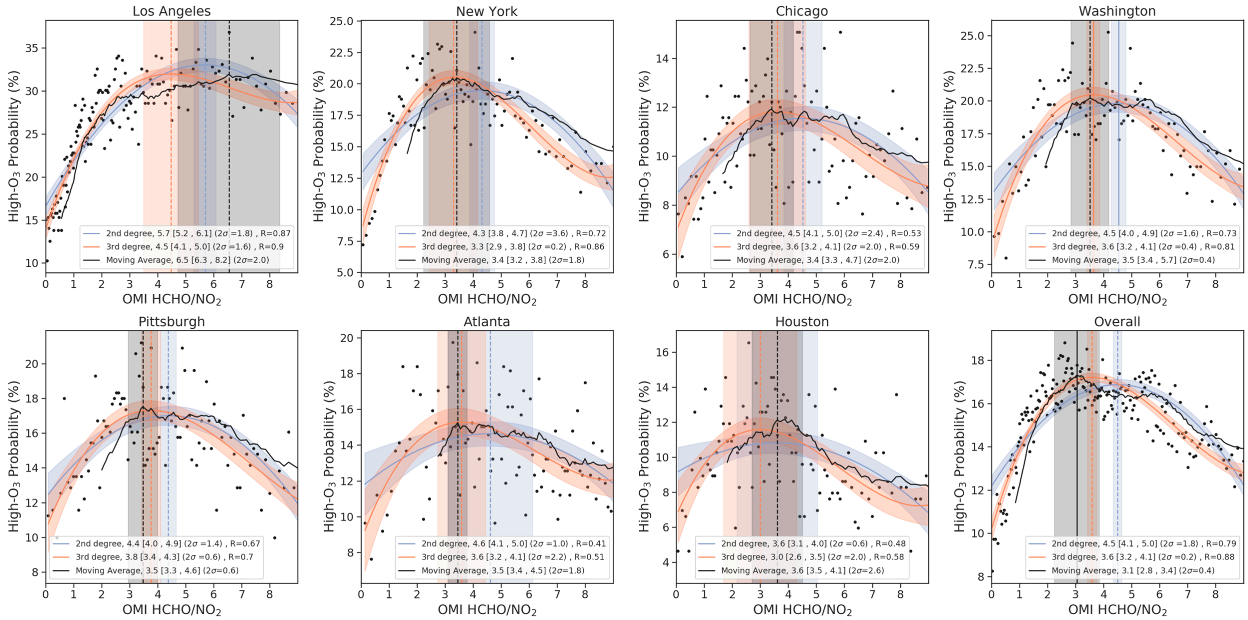

Figure S6. Same as Figure 1b but plotted with individual panels for seven cities and all sites combined using three models: (1) moving average (black), (2) 2[nd] degree polynomial model (blue), and (3) 3rd degree polynomial model (orange). R is the Pearson correlation coefficient between predictor and predicted values.

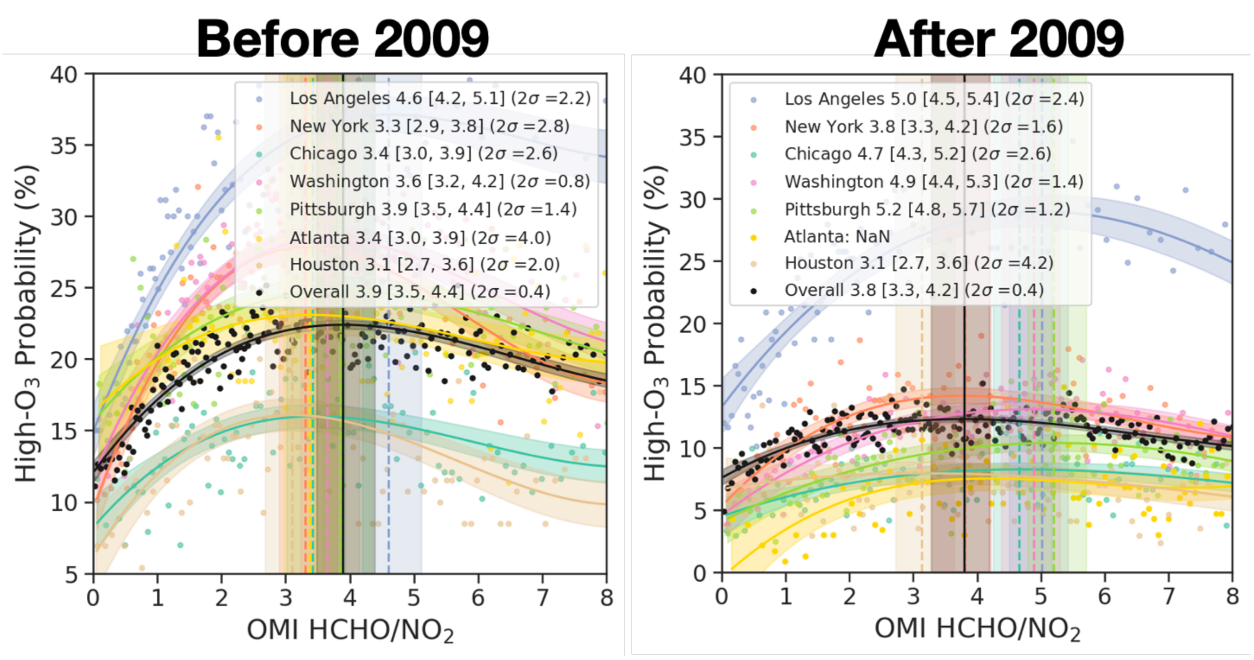

Figure S7. Same as Figure 1b but separated to two periods: before and after 2009.

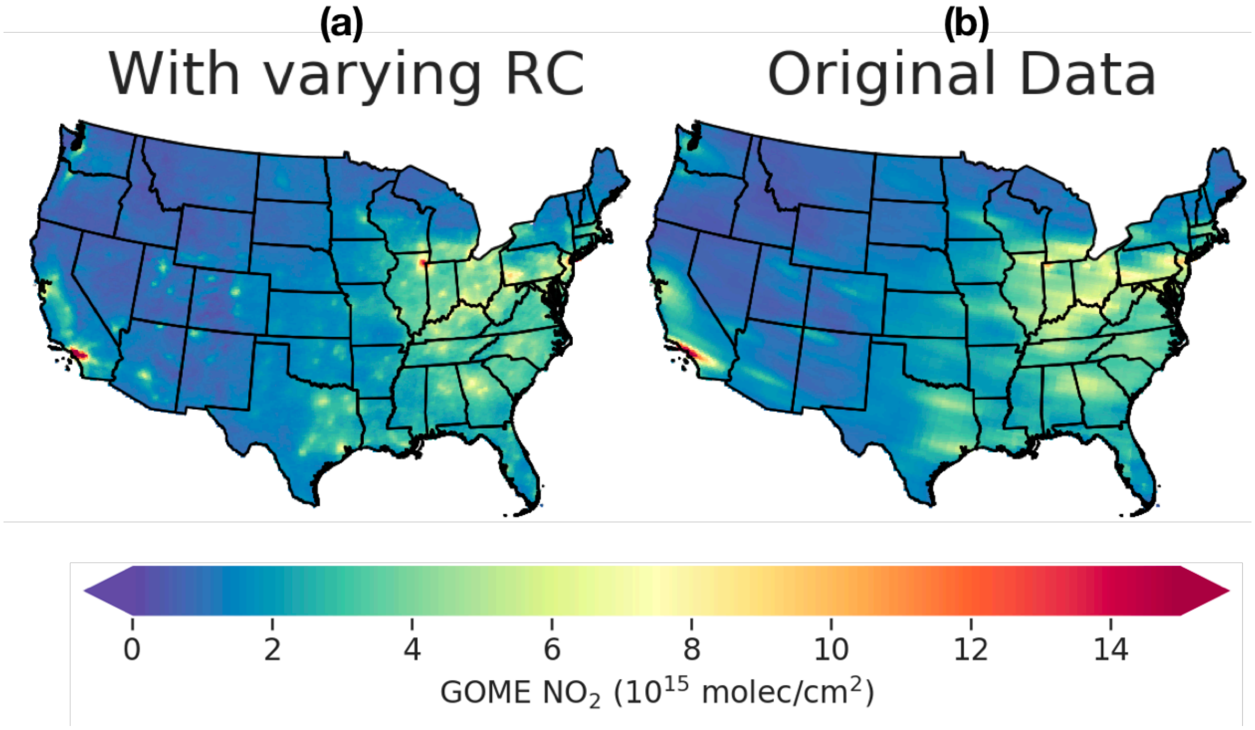

Figure S8. Summertime Ω_{NO2} averaged from 1996 to 2000 over the continental U.S.A. produced from (a) the harmonized GOME data using our new approach; (b) the original GOME satellite data.

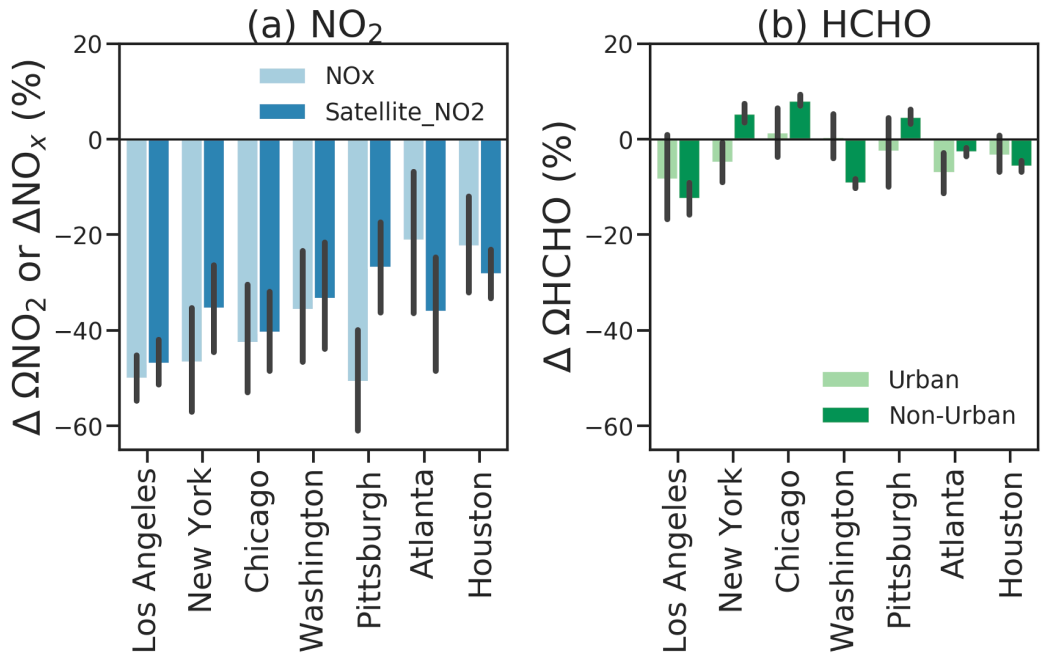

Figure S9. (a) Relative changes (%) in summertime average satellite-based Ω_{NO2} and the ground-based NO_x measurements in 1996 – 2000 versus 2013 - 2016 for seven cities. Satellite observations are sampled consistently over the locations with ground-based measurements of NO_x. We only include sites with at least 15 years observations available between 1996 and 2016. The underestimate of the relative change over Pittsburgh is caused by the low Ω_{NO2} in 1999, likely due to a retrieval issue. (b) Relative changes (%) in summertime average satellite-based Ω_{HCHO} over urban versus non-urban areas in 1996 – 2000 versus 2013 - 2016 for seven cities. The error bars indicate the spatial variation within each area. The separation of urban vs. non-urban areas is based on MODIS land cover type yearly Level-3 data in 2016 at 0.05° degree.[11]

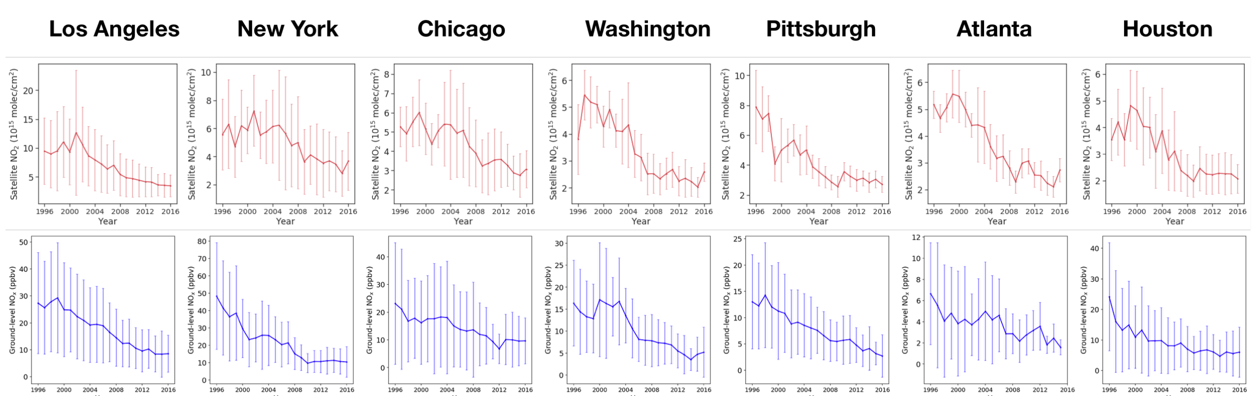

Figure S10. Time series of summertime satellite-based Ω_{NO2} (first row) and ground-based NO_x (second row) between 1996 to 2016 averaged for each Core-Based Statistical Area (CBSA). Satellite observations are sampled consistently over the locations with ground-based measurements of NO_x. We only select sites with at least 15 years of observations available between 1996 and 2016. The error bars show the spatial standard deviation across the region.

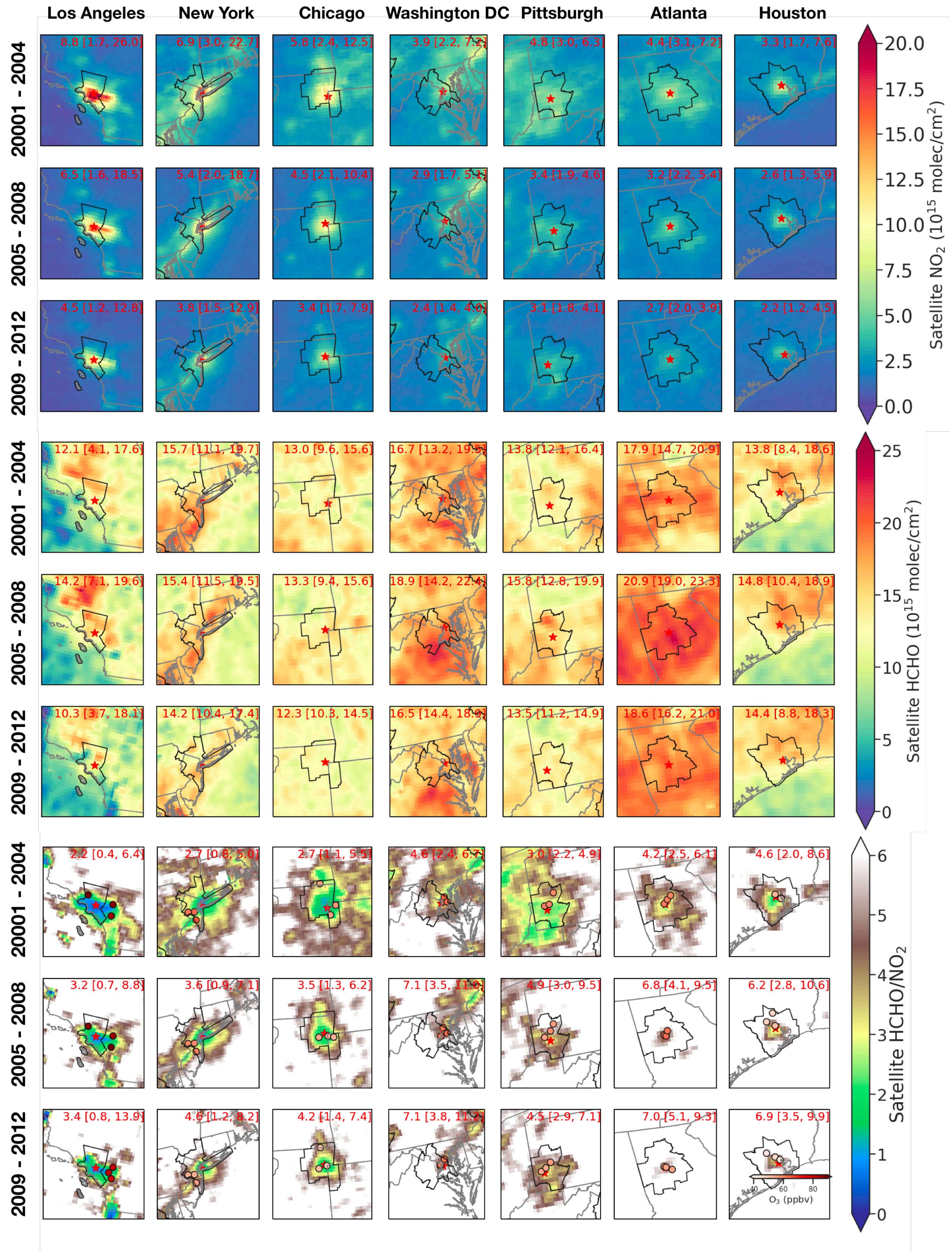

Figure S11. Same as Figure 2 but for 2001 – 2004, 2005 – 2008, 2009 – 2012.

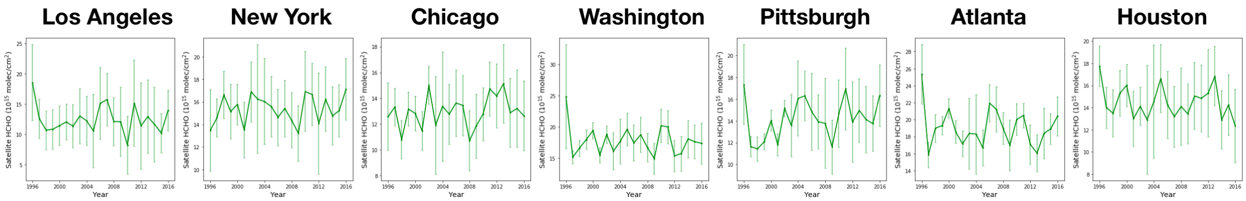

Figure S12. Time series of summertime satellite-based Ω_{HCHO} between 1996 to 2016 averaged for each CBSA. The error bars show the spatial standard deviation across the region.

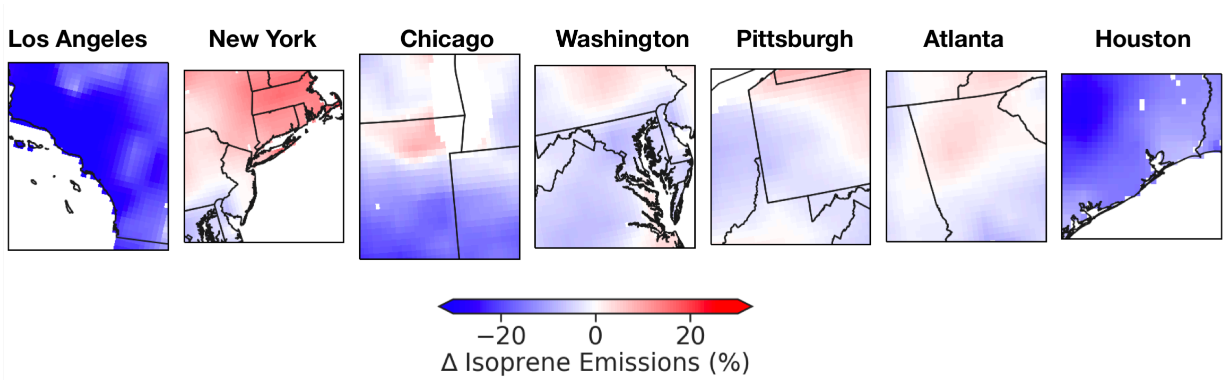

Figure S13. Maps of relative change in summertime isoprene emissions between 1996 – 2000 and 2013 – 2016. The isoprene emissions are generated with GEOS-Chem 12.3.0 using MEGAN2.1 driven by the MERRA2 meteorology at 0.5 ° × 0.625° resolution[12,13]. The data are accessed from http://geoschemdata.computecanada.ca/ExtData/HEMCO/OFFLINE_BIOVOC/v2019-10.

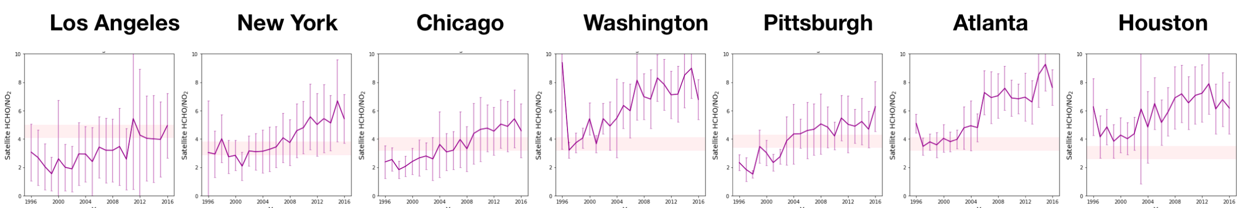

Figure S14. Time series of summertime satellite-based $HCHO/NO_2$ between 1996 to 2016 averaged for each CBSA. The error bars show the spatial standard deviation across the region. The pink bars indicate the transitional regimes derived from Figure 1b.

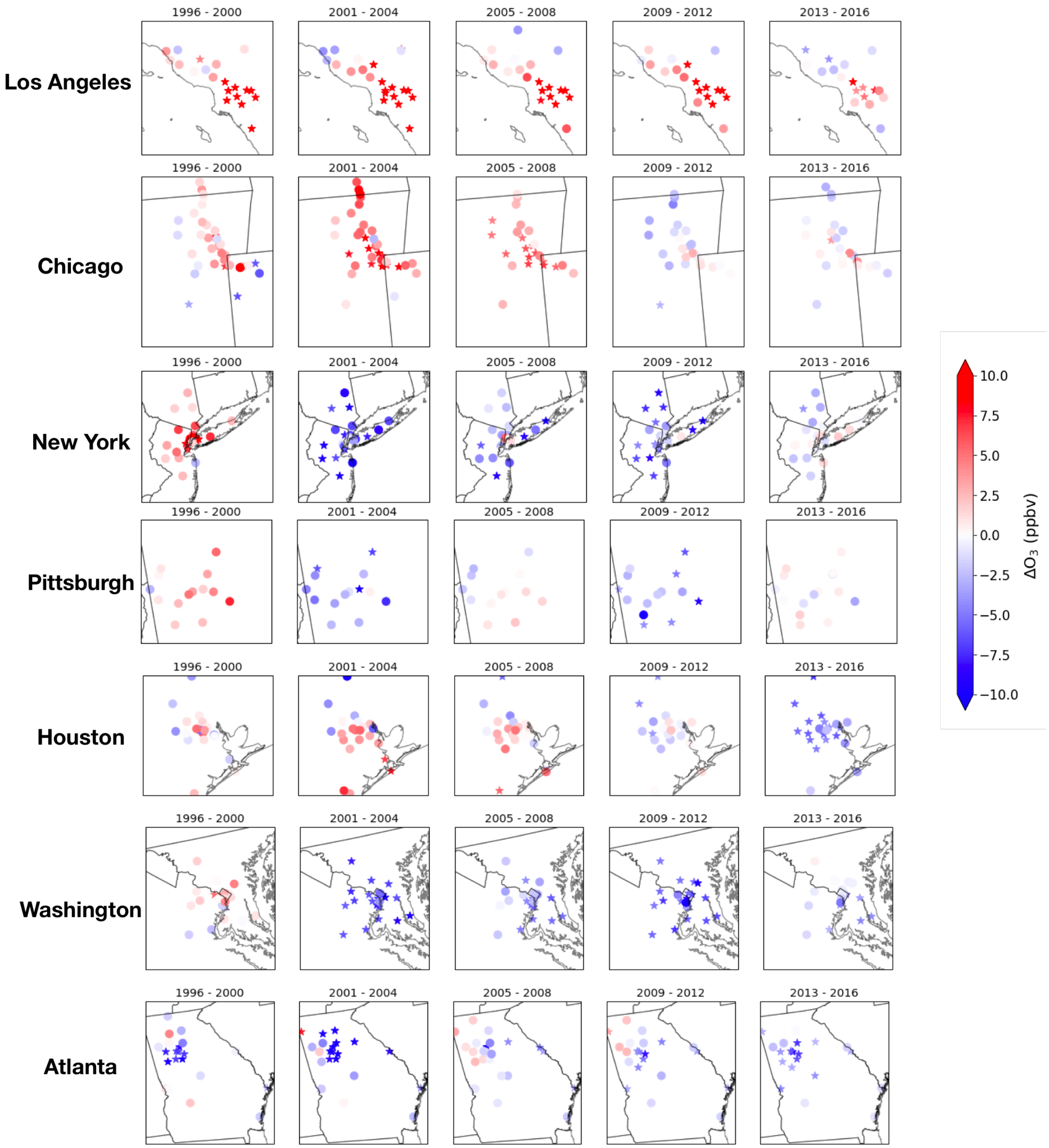

Figure S15. Weekday-to-weekend difference in AQS observed summertime average O_3 (weekend ΔO_3) in seven regions at high temperature (> median summer average temperature) during five periods 1996 – 2000, 2001 – 2004, 2005 – 2008, 2009 – 2012, 2013 – 2016). Sites with p<0.1 are labeled with stars, otherwise circles.

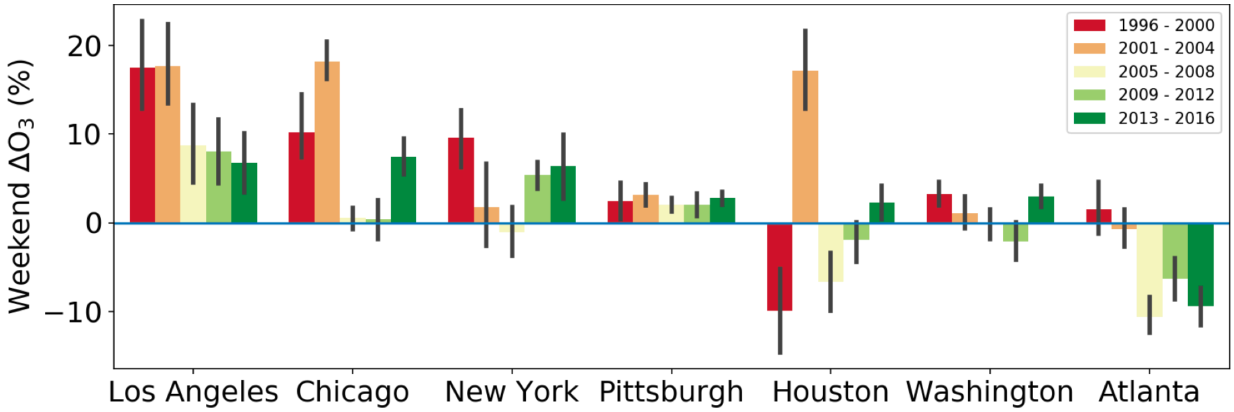

Figure S16. Same as Figure 5(b) but for moderate temperature (< median and higher than 18 ℃).

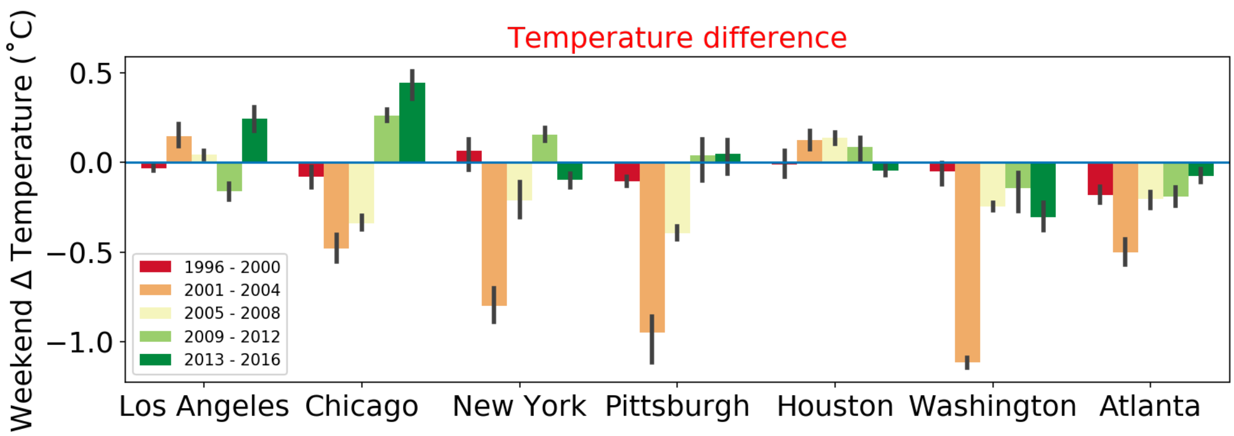

Figure S17. Weekday-to-weekend difference in average summertime temperature (weekend Δtemperature) in seven cities during five periods sampled over the ground-based sites. We use North American Regional Reanalysis temperature data at 10m.[14]

REFERENCES

(1) Platt, U.; Stutz, J. Differential Optical Absorption Spectroscopy; Springer Science & Business Media: Berlin, Heidelberg, 2008.

(2) Boersma, K. F.; Eskes, H. J.; Richter, A.; De Smedt, I.; Lorente, A.; Beirle, S.; van Geffen, J. H. G. M.; Zara, M.; Peters, E.; Van Roozendael, M.; et al. Improving algorithms and uncertainty estimates for satellite NO_2 retrievals: results from the quality assurance for the essential climate variables (QA4ECV) project. *Atmos. Meas. Tech.* **2018**, *11* (12), 6651–6678.

(3) Dirksen, R. J.; Boersma, K. F.; Eskes, H. J.; Ionov, D. V.; Bucsela, E. J.; Levelt, P. F.; Kelder, H. M. Evaluation of stratospheric NO_2 retrieved from the Ozone Monitoring Instrument: Intercomparison, diurnal cycle, and trending. *J. Geophys. Res.* **2011**, *116* (D8), 283–22.

(4) Williams, J. E.; Boersma, K. F.; Le Sager, P.; Verstraeten, W. W. The high-resolution version of TM5-MP for optimized satellite retrievals: description and validation. *Geosci. Model Dev.* **2017**, *10* (2), 721–750.
(5) Boersma, K. F.; Eskes, H. J.; Dirksen, R. J.; A, der, R. J. V.; Veefkind, J. P.; Stammes, P.; Huijnen, V.; Kleipool, Q. L.; Sneep, M.; Claas, J.; et al. An improved tropospheric NO_2 column retrieval algorithm for the Ozone Monitoring Instrument. *Atmos. Meas. Tech.* **2011**, *4* (9), 1905–1928.
(6) De Smedt, I.; Theys, N.; Yu, H.; Danckaert, T.; Lerot, C.; Compernolle, S.; Van Roozendael, M.; Richter, A.; Hilboll, A.; Peters, E.; et al. Algorithm theoretical baseline for formaldehyde retrievals from S5P TROPOMI and from the QA4ECV project. *Atmos. Meas. Tech.* **2018**, *11* (4), 2395–2426.
(7) Zara, M.; Boersma, K. F.; De Smedt, I.; Richter, A.; Peters, E.; van Geffen, J. H. G. M.; Beirle, S.; Wagner, T.; Van Roozendael, M.; Marchenko, S.; et al. Improved slant column density retrieval of nitrogen dioxide and formaldehyde for OMI and GOME-2A from QA4ECV: intercomparison, uncertainty characterisation, and trends. *Atmos. Meas. Tech.* **2018**, *11* (7), 4033–4058.
(8) McLinden, C. A.; Fioletov, V.; Boersma, K. F.; Krotkov, N.; Sioris, C. E.; Veefkind, J. P.; Yang, K. Air quality over the Canadian oil sands: A first assessment using satellite observations. *Geophys. Res. Lett.* **2012**, *39* (4).
(9) Zhu, L.; Jacob, D. J.; Keutsch, F. N.; Mickley, L. J.; Scheffe, R.; Strum, M.; Gonzalez Abad, G.; Chance, K.; Yang, K.; Rappenglück, B.; et al. Formaldehyde (HCHO) As a Hazardous Air Pollutant: Mapping Surface Air Concentrations from Satellite and Inferring Cancer Risks in the United States. *Environ. Sci. Technol.* **2017**, *51* (10), 5650–5657.
(10) Duncan, B. N.; Lamsal, L. N.; Thompson, A. M.; Yoshida, Y.; Lu, Z.; Streets, D. G.; Hurwitz, M. M.; Pickering, K. E. A space-based, high-resolution view of notable changes in urban NOx pollution around the world (2005-2014). *J. Geophys. Res. Atmos.* **2016**, *121* (2), 976–996.
(11) Friedl, M. A.; Sulla-Menashe, D.; Tan, B.; Schneider, A.; Ramankutty, N.; Sibley, A.; Huang, X. MODIS Collection 5 Global Land Cover: Algorithm Refinements and Characterization of New Datasets. *Remote Sensing of Environment* **2010**, *114* (1), 168–182. https://doi.org/10.1016/j.rse.2009.08.016.
(12) Guenther, A. B.; Jiang, X.; Heald, C. L.; Sakulyanontvittaya, T.; Duhl, T.; Emmons, L. K.; Wang, X. The Model of Emissions of Gases and Aerosols from Nature version 2.1 (MEGAN2.1): an extended and updated framework for modeling biogenic emissions. *Geosci. Model Dev.* **2012**, *5* (6), 1471–1492.
(13) Gelaro, R.; McCarty, W.; Suarez, M. J.; Todling, R.; Molod, A.; Takacs, L.; Randles, C. A.; Darmenov, A.; Bosilovich, M. G.; Reichle, R.; Wargan, K.; Coy, L.; Cullather, R.; Draper, C.; Akella, S.; Buchard, V.; Conaty, A.; Silva, A. M. da; Gu, W.; Kim, G.-K.; Koster, R.; Lucchesi, R.; Merkova, D.; Nielsen, J. E.; Partyka, G.; Pawson, S.; Putman, W.; Rienecker, M.; Schubert, S. D.; Sienkiewicz, M.; Zhao, B. The Modern-Era Retrospective Analysis for Research and Applications, Version 2 (MERRA-2). *Journal of Climate* **2017**, *30* (14), 5419–5454.
(14) Mesinger, F., G. DiMego, E. Kalnay, K. Mitchell, and Coauthors: North American Regional Reanalysis. *Bulletin of the American Meteorological Society*, **2006**, 87, 343–360, doi:10.1175/BAMS-87-3-343.